Increasing the load capacity of planar ferrofluid bearings by the addition of ferromagnetic material

Boots, A. S.T.; Krijgsman, L. E.; de Ruiter, B. J.M.; Lampaert, S. G.E.; Spronck, J. W.

Important note
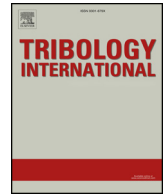To cite this publication, please use the final published version (if applicable).
Please check the document version above.

Increasing the load capacity of planar ferrofluid bearings by the addition of ferromagnetic material

A.S.T. Boots, L.E. Krijgsman, B.J.M. de Ruiter, S.G.E. Lampaert*, J.W. Spronck

Department of Precision and Microsystems Engineering, Delft University of Technology, Mekelweg 2, 2628CD, Delft, the Netherlands

ABSTRACT

Ferrofluid pocket bearings are a type of bearing that are able to carry a load using an air pocket encapsulated by a ferrofluid seal. Previously designed ferrofluid bearings show the great potential of the stick-slip-free and low viscous friction bearings, however until now the load capacity is limited. In this article a method is presented to increase the load capacity in a simple and cost effective way by the addition of ferromagnetic material around the magnet. First, a mathematical model of the bearing is presented and is validated by experiments using an axially magnetized ring magnet surrounded by two steel rings. The model is used to optimize the dimensions of the added ferromagnetic material for maximum load capacity. Depending on the fly height, the load capacity has been increased by a factor three to four by the addition of steel rings to the ferrofluid pocket bearing configuration.

1. Introduction

The kerosene based magnetic fluid or so called ferrofluid that NASA developed in the 1960s appeared to be interesting to apply in seals and bearings as shown by Rosensweig et al. in the 1970s [1–4]. A ferrofluid can be defined as a fluid with paramagnetic properties that are generated by being a colloidal suspension of small magnetic nanoparticles (10 nm) [5,6]. The application of an external magnetic field increases the pressure inside the fluid after which the fluid is capable of carrying loads [7–9], thus can act as an actuator [10–16] or seal [17–21]. Ferrofluid can be used to yield mechanisms that have complete absence of both stick slip and mechanical contact resulting respectively a potential high precision and high lifetime [7,8,22,23].

Because the fluid in ferrofluid bearings is contained by the presence of a magnetic field that is generated by for example a permanent magnet, no seals or active components are required. Therefore, a ferrofluid bearing is a passive, simple, and cost effective alternative to traditional bearings. Examples of these ferrofluid bearings can be found in literature, but despite the great potential, application is still very limited [7–9,24–29]. One reason for this is that the load capacity and stiffness is relatively limited. Lampaert et al. recently developed a mathematical model to describe the load and stiffness characteristics of ferrofluid bearings, which makes it now possible to design for maximum load capacity [7,8,22,23,26,30–33].

The load capacity of a ferrofluid bearing is created by the pressurized air pocket(s) encapsulated by the ferrofluid seals. The shape of the magnetic field and the number of air pockets between non-connected seals seem to be of great importance to the load capacity. The goal of this article is to increase the load capacity of ferrofluid bearings by the addition of ferromagnetic material.

The addition of ferromagnetic material, in this case steel, has the ability to concentrate the magnetic field generated by the permanent magnet and could therefore increase the load capacity [34,35]. Furthermore, steel could alter the shape of the magnetic field such that multiple air pockets can be created. Steel has a high magnetic saturation and a high relative permeability which makes this material suited for improving the load capacity.

First, a model is presented to calculate the load capacity of a ferrofluid double pocket bearing. This model is validated by experiments and will then be used to optimize the geometries of the steel rings. The acquired knowledge can be used as design rules for increasing the load capacity of planar ferrofluid bearings by the addition of ferromagnetic material.

2. Methods

First, an analytical model for the load capacity of a ferrofluid double pocket bearing is presented based on the available literature. Second, the four different bearing models, model A through D, are presented after which the FEM analysis, using COMSOL Multiphysics, is
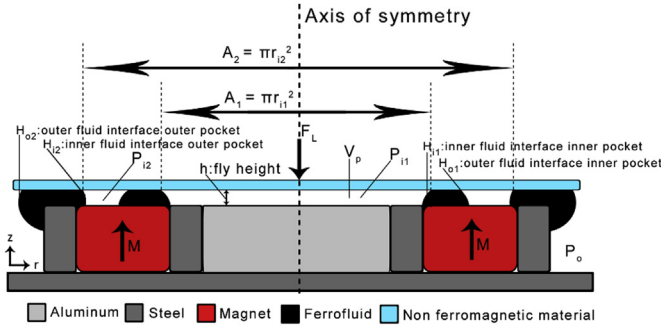

Fig. 1. This figure presents the cross section of the ferrofluid bearing with the defined parameters. The ring magnet is surrounded by two ferromagnetic rings, in this case steel, with an aluminum disk placed inside. The entire setup is mounted on a steel baseplate. Important parameters are the pressures and areas of the air pockets and the magnetic field intensities at the different fluid interfaces.

introduced to calculate the magnetic field intensities. These magnetic field intensities in combination with the analytical model are used to calculate the load capacity. Next, the experimental setup used for the validation of the described model is presented after which the optimizations of models A-D are described.

2.1. Analytical model

The analytical model for a ferrofluid single pocket bearing [8,9,24] is extended to a model predicting the load capacity of a ferrofluid double pocket bearing, schematically represented in Fig. 1. The Navier-Stokes equations for incompressible magnetic Newtonian fluids can be simplified to equation (1) assuming a stationary, low Reynolds number incompressible flow with a Newtonian fluid model. The relation presents the pressure gradient ∇p as the product of the magnetic permeability of vacuum μ_0, the magnetization strength of the fluid M_s and the magnetic field gradient ∇H.

$$\nabla p = \mu_0 M_s \nabla H \qquad 1$$

Application of the Fundamental theorem of calculus gives the relationship used for calculating the load capacity of the air pockets, equation (2).

$$F_{pocket} = \int_A (p_i - p_o) dA_{pocket} = \mu_0 M_S \, \Delta H \, A_{pocket} \qquad 2$$

Both the pressure inside the air pocket and the pressure inside the ferrofluid ring contribute to the total load capacity of the bearing. Although the load carrying contribution of the seal is relatively small in comparison to that off the pocket, it will be included in the calculation to get the most accurate prediction of the total load capacity. Equation (3) shows the approximation of the load capacity of the seal as described by Lampaert et al. [7].

$$F_{seal} = \int_A (p_s - p_0) dA_{seal} \approx \mu_0 M_S \, \Delta H \, \frac{A_{seal}}{3} \qquad 3$$

For a bearing configuration with two seals and two pockets the total load capacity is simply obtained by adding the load capacities of both pockets and both seals. Each contribution to the total load capacity is calculated by integrating the pressure difference over the area, as can be seen in equation (4). This is visually shown in Fig. 5, where the load capacities of the ferrofluid bearing for the magnet only and for the magnet with steel rings correspond to the orange and red surface respectively. The pressure distribution is a result of the magnetic field intensities of the fluid-air interfaces (H_{i1} H_{i2} H_{01} H_{02}), see Fig. 1. By integrating this pressure distribution, the total load capacity is calculated.

Implementation of a second ferrofluid seal has the advantage that the pressure can be increased twice, one time over each ferrofluid seal. It is important to note that the pressure contribution of the doughnut shaped second pocket, A_{p2}, as given in equation (4) can be rewritten to equation (5), in which the pressure contributions of both pockets act on a circular surface as defined in Fig. 1. To illustrate this, the pressure distribution which is given in Fig. 5 corresponds to the magnetic field intensities at the interfaces between ferrofluid and air, given in Fig. 4.

$$F_{load} = \int (p_{i1} - p_0) dA_{p1} + \int (p_{s1} - p_0) dA_{s1} + \int (p_{i2} - p_0) dA_{p2} + \int (p_{s2} - p_0) dA_{s2} \qquad 4$$

$$F_{load} \approx \mu_0 M_S \left((H_{i1} - H_{o1})\left(A_1 + \frac{A_{S1}}{3}\right) + (H_{i2} - H_{o2})\left(A_2 + \frac{A_{S2}}{3}\right) \right) \qquad 5$$
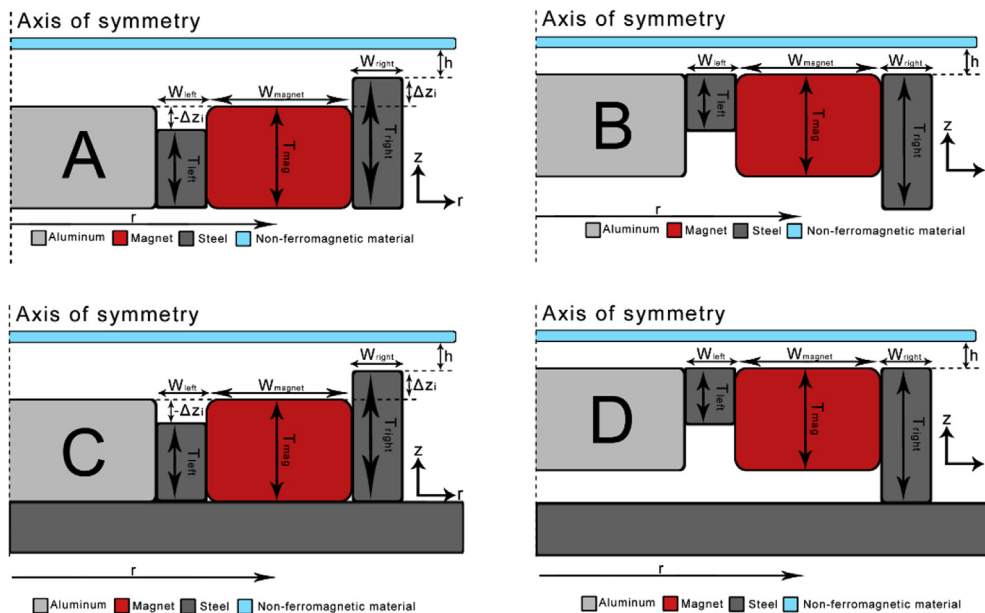

Fig. 2. This figure presents the four different bearing models and their design variables. In contrast to Model C and D, model A and B have no ferromagnetic baseplate. Model A and C are defined from bottom up and model B and D are defined from top down.

Table 1
This table presents a list of variables which are considered to be constant for the different bearing models A-D.

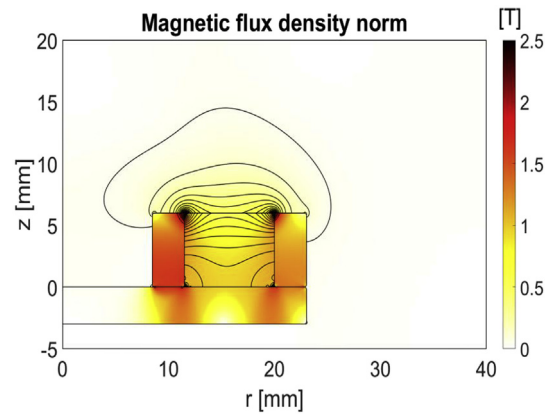| Optimization constants Optimization: Constants	
M_s	$= 35\,kA/m$
μ_0	$= 4\pi * 10^{-7}N/A^2$
W_{mag}	$= 8.5mm$
T_{mag}	$= 6mm$
T_{base}	$= 3mm$
h_{fly}	$= 0.2mm$
$B_{saturation,steel}$	$= 2.4T$
M_{magnet}	$= 1.25T$
p_0	$= 10^5 Pa$

Fig. 3. This figure presents the distribution of the magnetic field expressed in Tesla for the bearing testing setup of model C consisting of the ring magnet, steel rings and baseplate. The magnet is modelled after HKCM 9963–58947 with an axial magnetization strength of 1.25 T. The magnetic behaviour of the steel rings and baseplate is modelled in COMSOL using the built-in BH-curve of soft iron.
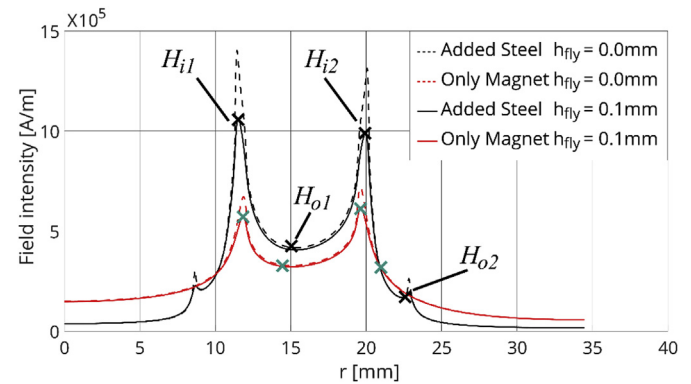
2.2. Bearing models

There are four distinct bearing models presented in this section, which will be referred to as model A, model B, model C and model D (Fig. 2). In all the models the ring magnet is sandwiched between two steel rings with varying widths and thicknesses. Both steel rings are attached to the magnet such that no volume exists between the steel rings and magnet.

The variables which are considered to be constant during the optimization of the bearing models A-D can be found in Table 1.

In model A the rings are fixed with respect to the bottom surface of the magnet. The thickness of the steel rings is defined with T_{left} and T_{right} and the width of the steel rings is defined with W_{left} and W_{right}. An additional parameter Δz_i is defined in equation (6), in which T_i indicates the thickness of the steel rings for either the left or right side.

$$\Delta z_i = T_i - T_{mag} \qquad\qquad 6$$

It can be concluded from the results of the model presented in section 3.2 that the top surface of the steel rings has to be at equal height as the surface of the magnet such that no steel protrudes beyond the thickness of the magnet. Therefore, model B is introduced. The steel rings are now fixed with respect to the top surface of the magnet and extended downwards.

To investigate the influence of a ferromagnetic baseplate on the load capacity, model C and D are introduced. Model C and D correspond to model A and B respectively, however with a 3 mm steel plate added. The baseplate is directly attached underneath the lowest part of the ferrofluid bearing (Fig. 2).

2.3. FEM analysis and load calculation

The magnetic fields generated by the different bearing configurations are calculated using the numerical analyses package COMSOL 5.3. The magnetic field intensity at the different fluid-air interfaces ($H_{i1}\ H_{i2}\ H_{01}\ H_{02}$) have to be evaluated in order to calculate the total load capacity according to equation (5).

The low grade steel of the rings surrounding the magnet is modelled by using the BH curve from the soft iron (with losses) material in the COMSOL library. Fillets are constructed at all the corners to prevent singularities in the calculations [36]. The model and the result of a single simulation example can be seen in Fig. 3 and Fig. 4. This example corresponds to model C as defined in Fig. 2. The bearing models are parameterized and controlled by Matlab (2017b) using the Livelink toolbox to find an optimal geometry.

The distribution of the magnetic field given in Fig. 3 is evaluated along a horizontal line at a specified height above the highest surface of the bearing, the so called fly height as defined in Fig. 1. An example of this line evaluation is given in Fig. 4 and is used to extract the magnetic strengths of the different interfaces. The ferrofluid will position itself at maximum load such that the inner fluid interfaces H_{i1} and H_{i2} are located at the maximum field intensities thus the peak values of Fig. 4.

Fig. 4. This figure presents the results of the FEM analysis for the magnetic field intensities, at 2 different fly heights, for the ring magnet (40 mm × 23 mm X 6 mm) with and without the addition of 3 mm × 6 mm steel rings. The magnetic flux density of the magnet is 1.25 T.

H_{01} is evaluated at the valley between the peaks in the middle of the magnet at a fly height of zero. When the value of H_{01} is bigger than either H_{i1} or H_{i2}, one seal and one air pocket is created. This comes from the fact that the fluid flows to the outer interface when the peak at a certain fly height is lower than the lowest value of the field intensity at the magnet (h= 0). The load capacity is then calculated with only the first part of equation (5). When both peaks are higher than the lowest field intensity at the magnet, two seals are created and both terms in equation (5) are taken into account. H_{o2} is evaluated at the fluid interface of the outer seal for a certain fly height. When the flyheight decreases, the ferrofluid seal is pushed outwards. For the magnet only, the outer interface of the ferrofluid seal increases from a radial distance of 21 mm–21.2 mm for fly heights of 1 mm–0 mm respectively. When steel rings are added, the radial distance of the outer interface remains 21.5 mm for a fly height of 1 mm, but increases to the radial distance of the outer steel ring at a fly height of 0 mm due to the steel rings. These values are observed experimentally and are interpolated linearly.

The radial position of the different field intensities are used to calculate the areas of the seals and the pockets. Finally, the load capacity of the bearing is calculated by combining the different field intensities with the corresponding areas and substituting this in equation (5).

To summarize, the FEM model (Fig. 3) is used to calculate the magnetic field produced by the magnet. This field is then evaluated to obtain the field intensities (Fig. 4), which can be used to calculate the
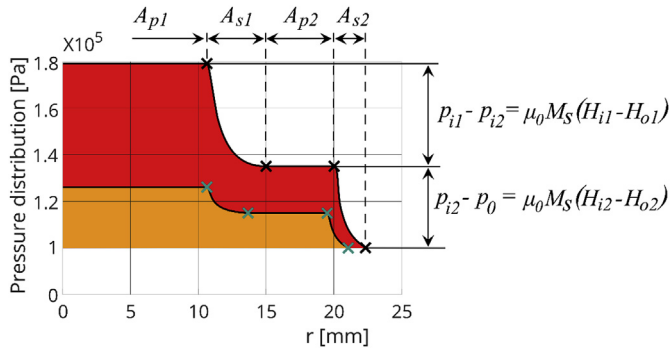
Fig. 5. This figure presents the pressure increase over the ferrofluid seals for both the magnet and the magnet with steel rings. The total load capacities for the magnet only and for the magnet with steel rings are indicated as the red and orange area resp. (For interpretation of the references to colour in this figure legend, the reader is referred to the Web version of this article.)

corresponding pressure distribution (Fig. 5) using the presented analytical model. Finally, the load capacity is obtained by integrating the pressure distribution of the area, indicated by the red area in the figure. Note that in Fig. 5 the pressure distribution and load capacity for the magnet only and for the magnet with steel rings are presented.

2.4. Experimental setup

The analytical model presented in section 2.1 is validated by comparing the predicted load capacity of the bearing with and without steel rings to the results of the measurements. Measurements are done to investigate the maximum load capacity of the bearing and validate the analytical model.

2.4.1. Load capacity

The maximum load capacity of the bearing with and without steel is measured using a tensile testing machine (Zwick/Roell Z005) capable of measuring the force over displacement. To prevent systematic errors, the machine is calibrated before measuring the load capacity. Each measurement is done three times to detect possible random errors. The velocity of the head of the testing machine is set to be 1 mm/min.

The bearing is mounted on top of a steel base plate, which corresponds to bearing model C (Fig. 2), and clamped on the table below the machine, see Fig. 6. Both the rings and the baseplate are made of low grade steel in the test setup, since the material is relatively cheap and has desirable ferromagnetic properties, which approximates the material used in the analytical model. There is assumed that the stiffness of the table is infinite with respect to that of the bearing. Moreover, the mounting is assumed to be rigid. Note that the volume inside the
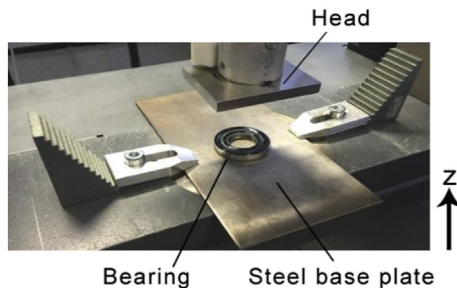

Fig. 6. This figure presents the bearing consisting of a ring magnet, two steel rings and ferrofluid. The ring magnet, HKCM 9963–58947 with dimensions 40 mm × 23 mm x6mm and a flux density of Bz = 1.25 T, is placed on a steel baseplate. This plate is clamped on the table and placed below the testing machine. 1 mL of ferrofluid is added to the bearing. The velocity of the head of the testing machine is set to be 1 mm/min.

magnet (and steel) in Fig. 6 is reduced by placing an aluminium cylinder inside. This is done in order to minimize the compressibility effect of air by reducing the volume of the inner air pocket [7]. Aluminium is chosen for its non-ferromagnetic properties, high stiffness and availability.

All the components are sealed and mounted with glue to prevent air leakage out of the two pockets. Then, 1 mL of FerroTec EFH1 is added. This amount of ferrofluid is redundant and can therefore create one or multiple air pockets and has a load carrying capacity up to fly heights of 1 mm.

The measurement of the load capacity starts just before the head of the testing machine touches the ferrofluid. No pressure can be build up across the seals at this point yet, because there are no separate air pockets and therefore no difference in magnetic field intensity across the ferrofluid seal ($\Delta H = 0$). The fly height is then decreased until the head of the testing machine starts pushing on the magnet itself. This indicates the end of the measurement of the load capacity.

2.5. Optimization

In this section the validated model, see results in section 3.1, will be used to optimize the geometry of the bearing models given in Fig. 2 for maximum load capacity. For the optimization, the fly height h is set to be 0.2 mm. The optimization of model A shows that the thickness of the steel rings should be equal to the thickness of the magnet, see results in section 3.2. Therefore, bearing model B is introduced. The configuration given in Fig. 2 of model B is optimized in a symmetric and asymmetric way. To investigate the influence of a ferromagnetic baseplate model C and D are introduced, as presented in section 2.2.

2.5.1. Optimization model A and C

The bearing models A and C presented in Fig. 2 will be optimized in both a symmetric and asymmetric configuration. The symmetric optimization is done in order to see the effect of the different variables on the load capacity of the bearing. Symmetric means in this case that the cross section of both steel rings have the same dimensions, thus $W_{left} = W_{right}$, $T_{left} = T_{right}$ and therefore $\Delta z_{left} = \Delta z_{right}$, as can be seen in Fig. 7. The design variables are normalized with respect to the dimensions of the magnet such that the results are easier to interpret. The normalizations are given in equations (7)–(9).

$$T_{ratio} = \frac{T_{steel}}{T_{mag}} \qquad\qquad 7$$

$$W_{ratio} = \frac{W_{steel}}{W_{mag}} \qquad\qquad 8$$

$$\Delta z_{ratio} = \frac{\Delta z}{T_{mag}} \qquad\qquad 9$$

This results in two design variables for the symmetric optimizations, namely: T_{ratio} and W_{ratio}. The design variables for the asymmetric
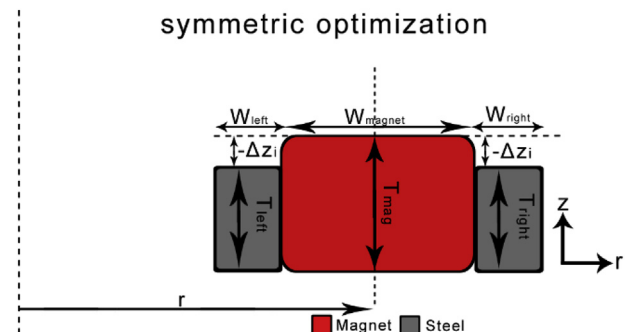

Fig. 7. This figure shows the variables for symmetric optimization and the cross sections of the steel rings.

optimizations for both models are: $T_{ratio-left}$, $W_{ratio-left}$, $T_{ratio-right}$, $W_{ratio-right}$. The Δz_{ratio} is introduced to investigate the height of the steel relative to the height of the magnet.

2.5.2. Optimization model B and D

The bearing models B and D, presented in Fig. 2, will be optimized in a symmetric and asymmetric way. The symmetric optimization is done in order to see the effect of the different variables on the load capacity of the bearing. Due to symmetry, $W_{left} = W_{right}$ and $T_{left} = T_{right}$. The design variables for the symmetric optimization of models B and D are reduced to: T_{ratio} and W_{ratio} and are defined in Fig. 7.

Finally, the asymmetric optimization is performed to see if introducing asymmetry in the system can further improve the load capacity. Note that all the different parameters are again normalized with respect to the magnet in the results. The design variables for the asymmetric optimization of models B and D are: $T_{ratio-left}$, $W_{ratio-left}$, $T_{ratio-right}$, $W_{ratio-right}$, as defined in Fig. 2.

2.5.3. Optimization algorithm

To find an optimum for the configurations described above, an algorithm is designed. The algorithm can be seen as a multi-point approximation method. It evaluates a certain preset subdomain of the design space. The optimal point of the subdomain is considered to be the midpoint of the next subdomain in the next cycle. The process can be seen in Fig. 8. In the asymmetric optimization of the steel rings, this results in a 4D subdomain, consisting of all the design variables. This algorithm solves the optimization problem and is convenient since the function evaluations ask a lot of computational effort.

A subdomain is built using its midpoint, the length of the subdomain and the number of samples. The side length of the subdomain is chosen such that the dimensions of steel increase from no steel rings up to the inner side of the magnet completely filled with steel. Then the subdomain is evaluated and the minimum value is determined. To achieve convergence, the size of the new subdomain must be smaller than that of the previous one. Therefore, the length of each side of the new trust region is scaled. Scaling (< 1) of the subdomain makes the algorithm converge to a certain optimum. The scaling number is determined iteratively by varying this number. A small scaling number makes the subdomain converge too fast and the optimal value is not found ($S < 0.4$). A larger scaling number result in more iterations, but the optimum is found ($0.4 < S < 0.1$).

3. Results

3.1. Load capacity

The load capacity has been analytically calculated and
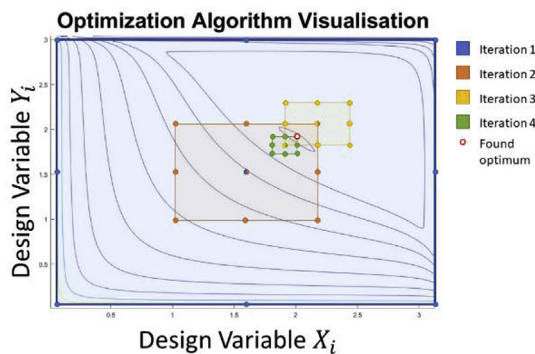

Fig. 8. This figure presents the way the optimization algorithm works. In the first step the entire domain is considered in which 9 points are evaluated. The best point will be the centre of the next iteration step in which the domain will be smaller. These steps will be repeated until an optimum is found.
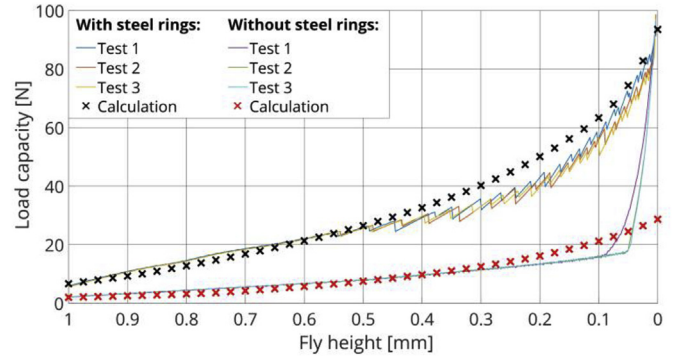

Fig. 9. This figure presents the load capacity predicted by the analytical model and measured by the testing machine versus different fly heights for the magnet only and the magnet with 3 mm wide inner and outer steel rings that have the same z-position as the magnet.

experimentally measured for both the single magnet and the magnet with steel rings for several fly heights. These results can be seen in Fig. 9. The results of the different experiments are indicated with continuous lines while the calculations are indicated with crosses.

Notable is that adding a 3 mm wide inner and outer ring of steel improves the load capacity of the bearing at fly height 0.2 mm with approximately a factor 4. For higher fly heights this factor ranges approximately from 3 to 4. This is a significant improvement compared to the ferrofluid pocket bearing without the steel rings. Also note the zig-zag pattern in the measurements for the improved bearing at lower fly heights.

The overall behaviour of the load capacity of the improved bearing is predicted well by the calculations and both the model and measurements are in good accordance with each other.

3.2. Optimization

The results of the optimization of model A are given in Fig. 10. From this plot it can be concluded that the load capacity is the highest for $\Delta z = 0$ mm for all the different normalized widths of the steel rings. Note that the load capacity significantly decreases if Δz_{ratio} deviates from zero.

The results of the symmetric optimization of model B are given in Fig. 11, Figs. 12 and 13. Fig. 11 shows the load capacity for the two design variables in a single surface plot. Figs. 12 and 13 show side views or cut troughs of the surface plot in Fig. 11.

Fig. 13 shows that the T_{ratio} needs to be approximately 1.2 or higher. The load capacity decreases significantly when the T_{ratio} decreases. In combination with Fig. 13 this leads to the conclusion that for a
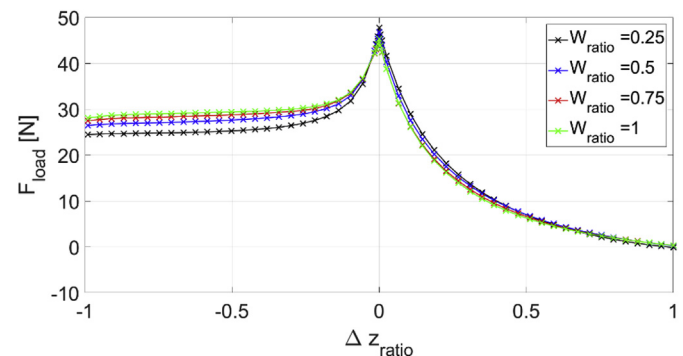

Fig. 10. This figure presents the load capacity of the ferrofluid bearing with additional steel rings for varying thicknesses and widths of the rings. These dimensions are normalized with respect to the thickness and width of the magnet.
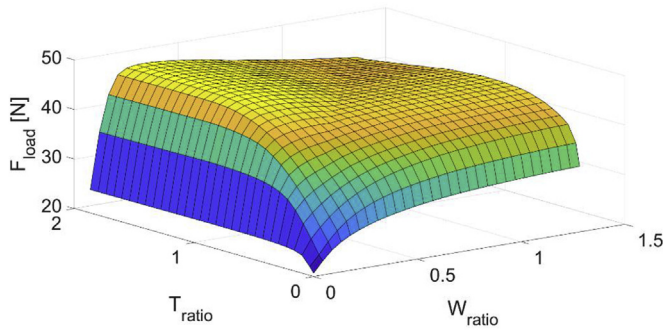
Fig. 11. This figure presents a surface plot of the load capacity of model B with varying dimension parameters H_{ratio} and W_{ratio}.
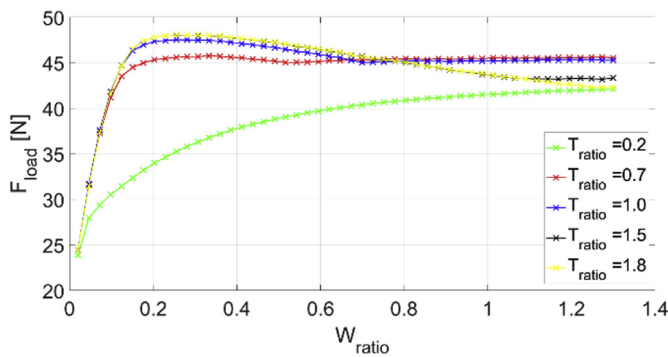

Fig. 12. This figure presents the load capacity of model B versus W_{ratio} for different H_{ratio}.
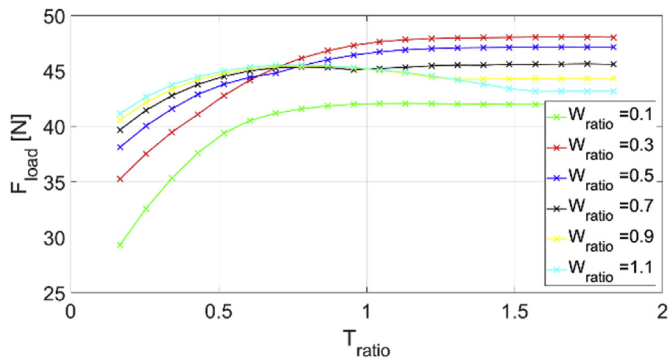

Fig. 13. This figure presents the load capacity of model B versus H_{ratio} for different W_{ratio}.

symmetric configuration of steel rings without baseplate the maximum load capacity of approximately 48N is achieved for $T_{ratio} \approx 1.8$ and $W_{ratio} \approx 0.26$.

The results of the symmetric and asymmetric optimization of model A, B, C and D are given in Table 2. It can be concluded that the addition of the ferromagnetic baseplate changes the optimal geometry of the added ferromagnetic rings as can be seen in Figure 14. Furthermore, when the baseplate is added, an additional 3 N ($\approx$ 6%) increase in load capacity can be obtained.

A visual representation of the optimized bearing configurations for the bearing models is given in Figure 14. The dimensions of the steel rings and the load capacities can be found in Table 2.

4. Discussion

4.1. Analytical model and measurements

Overall, the measurements show that the load capacity of the ferrofluid double pocket bearing is increased 3 to 4 times depending on the fly height by the addition of steel rings around the ring magnet. Addition of these ferromagnetic rings increases the difference in magnetic field intensities over the ferrofluid seal. This increase has the advantage that capillary effects can be overcome such that two air pockets are created. Both the increase in difference in field intensities and the addition of the second seal contribute to the total load capacity, leading to an increase of a factor 4.

The measured load capacity of the bearing with and the bearing without steel rings correspond well to the calculated load capacity. However, the calculations do slightly differ from the actual measurements for both models. From the results it can be seen that at lower fly heights the load capacity for both models is overestimated. This overestimation is probably due to the fact that capillary effects are not taken into account in the mathematical model. Moreover, these capillary effects increase when the fly height decreases.

Also for a magnet with steel rings, the load capacity is overestimated. It seems that the capillary effects are overcome and two seals are formed. However, for low fly heights, the ferrofluid is pushed outwards too far due to the steel rings and do not participate in the load capacity anymore. Therefore, the volume of effective ferrofluid decreases during the measurements, leading to an overestimation of the load capacity. When the amount of effective ferrofluid is overestimated, the realistic value of the H_{o1} is not the lowest value for the field intensity at the magnet and is therefore not located at the valley. The outer interface of the ferrofluid will be located at a higher field intensity, leading to a lower load capacity.

On top of that, the steel rings are modelled in COMSOL as soft iron. In reality, there will be a difference in material properties between the steel rings and the material used in the model. The overall behaviour/ shape of the predicted load capacity of the bearing with steel does correspond well to the measurements, and therefore the model can be seen as valid and is used for optimization. It is likely that finding a better BH curve will reduce the overestimation of the load capacity. Another possible error in the FEM model is the applied radius of the fillets, which might also differ from the actual fillets of the steel rings and magnet used in the experimental setup. Note that in general the FEM model starts to become unreliable when the fly height is approaching zero. This is due to effects in the FEM analysis near boundaries and corners of the magnet.

When the fly height is decreased in the measurements, the assumed incompressible ferrofluid is pushed outwards. The fluid-air interfaces get displaced outwards, this increases the areas of the seals and changes the magnetic field intensities at the different interfaces. These effects are included in the analytical and numerical model. In the model, the most outer interface is assumed to linearly increasing from a radial distance of 21 mm–21.2 mm and 21 mm to the radial distance of the edge of the outer steel ring for the magnet only and the magnet with steel rings respectively. Implementation of a more realistic gradient in this outer interface will probably yield better results.

When the fly height is decreased the air pressure inside the pockets increases until the point that the seals cannot withstand the pressure anymore. Air escapes out of the pocket and causes the ripples or zig-zag pattern in the measurements in Fig. 9.

4.2. Optimization model A and C

When the W_{ratio} is (very) small there is simply very little steel added to the bearing resulting in that the influence of the steel on the magnetic field is almost negligible. To prevent instant saturation, the W_{ratio} has to be higher than a certain value. Approximately a W_{ratio} of 0.3

Table 2

This table presents the overview of the optimization of the load capacities for the different bearing models discussed in this article **without and with** baseplate.

Model		Design variables				Field intensities				Result
		$T_{ratio-left}$	$W_{ratio-left}$	$T_{ratio-right}$	$W_{ratio-right}$	$H_{i1} \begin{bmatrix} \times 10^5 \\ A/m \end{bmatrix}$	$H_{o1} \begin{bmatrix} \times 10^5 \\ A/m \end{bmatrix}$	$H_{i2} \begin{bmatrix} \times 10^5 \\ A/m \end{bmatrix}$	$H_{o2} \begin{bmatrix} \times 10^5 \\ A/m \end{bmatrix}$	**LOAD CAPACITY** [N]
A	Symmetric	1	0.27	1	0.27	8.268	3.652	7.581	1.486	47.29
	Asymmetric	1	0.24	1	0.29	8.238	3.648	7.585	1.417	47.65
B	Symmetric	1.8	0.26	1.8	0.26	8.53	3.708	7.692	1.547	48.06
	Asymmetric	1.71	0.27	1.71	0.31	8.500	3.702	7.700	1.5	48.31
C	Symmetric	1	0.37	1	0.37	8.835	4.225	8.198	1.420	51.19
	Asymmetric	1	0.35	1	0.37	8.822	4.224	8.203	1.420	51.20
D	Symmetric	1	0.37	1	0.37	8.835	4.225	8.198	1.420	51.19
	Asymmetric	1	0.35	1	0.37	8.822	4.224	8.203	1.420	51.20

balances complete magnetic saturation and diffusion of the magnetic field into the steel when the width of the steel rings becomes to large.

Regardless of the width of the steel rings, the thickness of the steel rings has to be equal to the thickness of the magnet to obtain the maximum load capacity (section 3.2). When the thickness of the steel rings is less than that of the magnet, the magnetic field is less concentrated at a fly height just above the magnet because the field lines have to travel a greater distance through the air to close the magnetic circuit using the steel. Also due to the low relative permeability of air, the magnetic field lines diffuse into the air, which lowers the load capacity. On the other hand, when the thicknesses of the ferromagnetic rings are higher than the magnet, the fly height is defined as the distance between the non-ferromagnetic plate and the top of the steel rings instead of the magnet (Fig. 2). The magnetic field will in this case be concentrated within the volume above the magnet and between the steel rings surrounding the magnet while the load capacity is determined by the fly height above the steel rings where the magnetic field is much weaker. Therefore, taking the thickness of the steel rings smaller than that of the magnet is less detrimental to the total load capacity of the ferrofluid bearings than taking the thickness too big.

Besides that, steel rings with the same thickness as the magnet have the advantage that the flat top prevents the ferrofluid from dripping down. In this way, the ferrofluid can be used in an optimal way since the ferrofluid seal is able to span a greater horizontal length which increases the load capacity since the difference in magnetic field increases between both interfaces ($\Delta H = H_i - H_0$).

4.3. Optimization model B and D: symmetric

When the T_{ratio} is (very) small there is simply very little steel added to the bearing resulting in that the influence of the steel on the magnetic field is almost negligible, see Fig. 12. The magnetic field has to travel through the air instead of the added steel. Therefore, increasing the thickness of the steel rings increases the load capacity significantly until a T_{ratio} of 1.2 is reached for the bearing without baseplate (model B). For a T_{ratio} of 1, the thickness of the steel rings and the magnet are equal. In this case, the magnetic field leaves the steel and has to make a 180° turn through the air to close the magnetic circuit. Steel rings which are slightly thicker than the magnet reduce this turn to 90°. Therefore a T_{ratio} of at least 1.2 results in the highest load capacity. Further increasing the thickness of the steel beyond a ratio of 1.2 has no influence on the load capacity since the magnetic field does not protrude into the added steel since this would increase the path by the magnetic field lines to close the magnetic circuit. When a baseplate is added below the bearing the thickness of the steel rings has to be equal to the thickness of the magnet.

This can be explained by looking at the magnetic properties of the added material. Once the width of the rings is too small, magnetic saturation of the rings occurs which can be seen in Fig. 12. After the ferromagnetic material is saturated, the magnetic field is not influenced by the material anymore. Therefore, the magnetic saturation of the ferromagnetic material limits the load capacity. Increasing the width increases the load capacity. However, when the width of the rings is too large, the field lines are not concentrated at the edges of the magnet where the ferrofluid will be placed, but distributed into the steel rings,
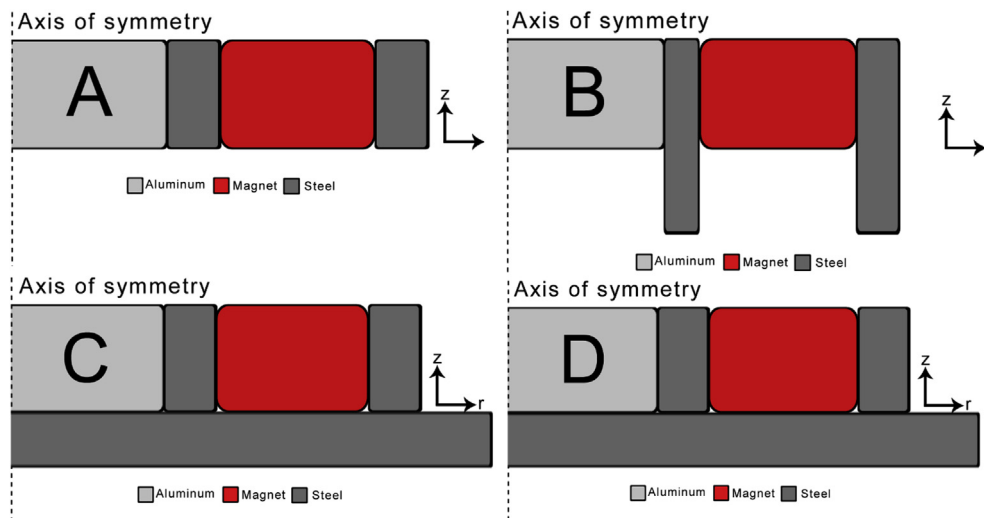

Fig. 14. This figure presents the optimal bearing configurations to achieve maximum load capacity for the ring magnet sandwiched between steel rings without being placed on top of a baseplate (model A and B) and placed on top of a baseplate (model C and D).

which decreases the load capacity. When the width of the rings is increased even further, the dispersion does not increase and therefore the load capacity remains constant which explain the behaviour in Fig. 12 for increasing widths of the steel rings.

Therefore, it can be concluded that the steel needs to have a certain minimum width to prevent magnetic saturation. The optimal width of the rings for the symmetric model B is $W_{ratio} = 0.26$ which balances the magnetic saturation and dispersion of the magnetic field. When a baseplate is added (Model D) the rings need to be a little bit wider (Table 2), namely $W_{ratio} \approx 0.37$. Note that when the inner ring is increased such that the magnet is completely filled with steel, the magnetic field is short circuited and the load capacity decreases.

4.4. Optimization model B and D: asymmetric

The optimal thickness of the rings in the asymmetric optimization of model B happens to be symmetric, namely $T_{ratio} = 1.71$ for the bearing without baseplate, see Table 2. The thickness of the rings exceeds the thickness of the magnet such that it is easier for the magnetic field to close the magnetic circuit. Only a turn of 90° is required for the magnetic field when it leaves the steel ring instead of a full 180° turn. When an additional ferromagnetic baseplate is added the optimal thickness of the rings is equal to the thickness of the magnet which is quite convenient when mounting the bearing. This way the entire magnet is surrounded by steel except for the top surface where the ferrofluid is placed. Besides that the addition of the baseplate changes the optimal thickness significantly such that the bearing can be mounted much more easily, the load capacity is increased by approximately $3N$ ($\approx 6\%$) therefore it is recommended to choose the thickness of the rings equal to the thickness of the magnet and to mount the bearing on a ferromagnetic baseplate.

The optimal width for the steel rings also depends on the presence of a baseplate. As earlier mentioned, a certain minimum value for the width is required to prevent magnetic saturation. If the width is too large the concentration of the magnetic field is decreased which decreases the load capacity but this effect is not as detrimental as the magnetic saturation of the steel. When a baseplate is present, the optimal widths of the steel rings is slightly bigger with respect to a bearing without baseplate, namely $W_{ratio} \approx 0.27$ (model A) & $W_{ratio} \approx 0.26$ (model B) versus $W_{ratio} \approx 0.37$ (model C) & $W_{ratio} \approx 0.37$ (model D) respectively. Introducing asymmetry into the system only increases the load capacity marginally (0.1%) and one can therefore argue whether it is worth the trouble to implement this in practice.

The load capacity can even be increased further if the strength of the magnet and the magnetic saturation of the ferromagnetic material are increased. A larger magnet (a larger T_{mag} or W_{mag}) has a bigger volume and therefore higher magnetic field intensities which increases the load capacity. This is not investigated in this article since it is not a cost effective way to increase the load capacity. Also, a stronger magnet results in an increase of the optimal width of the rings in order to prevent complete magnetic saturation. Increasing the magnetic saturation of the ferromagnetic material does exactly the opposite, namely resulting in a smaller optimal width. This comes from the fact that less material is needed to prevent saturation. Thus, choosing materials with better magnetic properties for the rings can increase the load capacity of the described ring magnet even more. However, using different ferromagnetic materials than steel could increase the costs, which makes the increase in load capacity by adding a ferromagnetic material less cost effective. These and many other possible improvements are not discussed in this article since the goal was to increase the load capacity of a ferrofluid bearing in a cheap and easy manner.

5. Conclusion

The experiments show that the model is in good accordance for the bearing with and without the ferromagnetic rings.

Overestimation of the load capacity is probably caused by capillary effects, an overestimation of the amount of effective ferrofluid and a mismatch between the modelled magnetic saturation and the actual material properties of the steel used in the test setup. The bearing furthermore shows excellent repeatability after an initial compression.

The addition of steel rings does not only increase the differences in field intensities, but also gives the opportunity to overcome the capillary effects and give rise to a second seal. Therefore, it can be concluded that the load capacity of the ferrofluid pocket bearing can be improved by the addition of steel rings up to a factor of 3–4, depending on the fly height and the dimensions of the steel.

Optimization shows that the maximum load capacity is reached if the thickness of the steel is equal to the thickness of the magnet and if the bearing is mounted on a ferromagnetic baseplate. Moreover, the optimal width depends on the magnetic saturation of the rings and the strength of the magnet. Ideally, the rings are on the verge of being completely saturated which optimally concentrates the magnetic field at the corners of the magnet. The optimal width of the steel for the ring magnet described in this report is approximately a third of the width of the magnet.

Acknowledgments

References

[1] Rosensweig R. Bearing arrangement with magnetic fluid defining bearing pads. 1971. 3 612 630.
[2] Rosensweig R. Magnetic fluid seals. 1971.
[3] Papell S. Low viscosity magnetic fluids obtained by the colloidal suspension of magnetic particles. 1965. 3 215 572.
[4] Rosensweig RE. Non-bursting ferrofluid seal. 2001. US6543782B1.
[5] Rosensweig RE. Ferrohydrodynamics. Dover Publications Inc; 2013.
[6] Rinaldi C, Chaves A, Elborai S, He X, Zahn M. Magnetic fluid rheology and flows. Curr Opin Colloid Interface Sci 2005;10:141–57. https://doi.org/10.1016/j.cocis.2005.07.004.
[7] Lampaert SGE, Spronck JW, van Ostayen RAJ. Load and stiffness of a planar ferrofluid pocket bearing. Proc Inst Mech Eng Part J J Eng Tribol 2017. https://doi.org/10.1177/1350650117739200. 135065011773920.
[8] Lampaert SGE, Fellinger BJ, Spronck JW, Ostayen RAJ Van. In-plane friction behaviour of a ferrofluid bearing. Precis Eng 2018https://doi.org/10.1016/j.precisioneng.2018.05.013.
[9] Lampaert SGE. Modelling and Design Principles of planar ferrofluid bearings. DSPE-Conference. 2016 2016.
[10] Cheng HC, Xu S, Liu Y, Levi S, Wu ST. Adaptive mechanical-wetting lens actuated by ferrofluids. Optic Commun 2011;284:2118–21. https://doi.org/10.1016/j.optcom.2010.12.073.
[11] Uhlmann E, Bayat N. High precision positioning with ferrofluids as an active medium. CIRP Ann - Manuf Technol 2006;55:415–8. https://doi.org/10.1016/S0007-8506(07)60448-X.
[12] Torres-Díaz I, Rinaldi C. Recent progress in ferrofluids research: novel applications of magnetically controllable and tunable fluids. Soft Matter 2014;10:8584–602. https://doi.org/10.1039/C4SM01308E.
[13] Sudo S, Takaki Y, Hashiguchi Y, Nishiyama H. Magnetic fluid devices for driving micro machines. JSME Int J Ser B 2005;48:464–70. https://doi.org/10.1299/jsmeb.48.464.
[14] Olaru R, Petrescu C, Hertanu R. A novel double-action actuator based on ferrofluid and permanent magnets. J Intell Mater Syst Struct 2012;23:1623–30. https://doi.org/10.1177/1045389X12449916.
[15] Liu Q, Alazemi SF, Daqaq MF, Li G. A ferrofluid based energy harvester: computational modeling, analysis, and experimental validation. J Magn Magn Mater 2018;449:105–18. https://doi.org/10.1016/j.jmmm.2017.09.064.
[16] Jayhooni SMH, Assadsangabi B, Takahata K. A stepping micromotor based on ferrofluid bearing for side-viewing microendoscope applications. Sensors Actuators, A Phys 2018;269:258–68. https://doi.org/10.1016/j.sna.2017.11.020.
[17] Mitamura Y, Takahashi S, Amari S, Okamoto E, Murabayashi S, Nishimura I. A magnetic fluid seal for rotary blood pumps: effects of seal structure on long-term performance in liquid. J Artif Organs 2011. https://doi.org/10.1007/s10047-010-0526-8.
[18] Ravaud R, Lemarquand G, Lemarquand V. Mechanical properties of ferrofluid applications: centering effect and capacity of a seal. Tribol Int 2010. https://doi.org/10.1016/j.triboint.2009.04.050.
[19] Yang R, Hou H, Wang Y, Fu L. Sensors and Actuators B : Chemical Micro-magnetofluidics in microfluidic systems : A review vol. 224. 2016. p. 1–15.
[20] Potma OGR. To. Designs for rotary shaft fluid seals in an aqueous environment

using ferroflui vol. 98. 2017.

[21] Urreta H, Aguirre G, Kuzhir P, Lopez de Lacalle LN. Seals based on magnetic fluids for high precision spindles of machine tools. Int J Precis Eng Manuf 2018. https://doi.org/10.1007/s12541-018-0060-9.

[22] Lampaert SGE, Spronck JW, van Ostayen RAJ, Café M. (2 + 4) DOF precision motion stage with ferrofluid bearings department of precision and microsystems engineering delft university of technology. 5–8. 2014.

[23] Café M. Nanometer precision six degrees of freedom planar motion stage with ferrofluid bearings. Technical University Delft; 2014.

[24] Lampaert SGE. Planar ferrofluid bearings modelling and design principles. Technical University Delft; 2015.

[25] Lampaert SGE, Spronck JW, van Ostayen RAJ. Hydrostatic bearing with MR texturing. B abstr 16th ger ferrofluid work. 2017. p. 94–5.

[26] Lampaert SGE, Spronck JW, van Ostayen RAJ. Load & stiffness of a planar ferrofluid pocket bearing S.G.E. 17th nord symp Tribol 2016. https://doi.org/10.1017/CBO9781107415324.004.

[27] Lampaert SGE, Spronck JW, van Ostayen RAJ. Virtual textured hybrid bearings. 44th Leeds-Lyon Symp. Tribol 2017;30:84.

[28] Millet G, Hubert A. Design of a 3 DOF displacement stage based on ferrofluids. Actuators 2006;06:656–9.

[29] Alvarez-Aguirre A, Mok G, HosseinNia SH, Spronck J. Performance improvement of optical mouse sensors: application in a precision planar stage. 2016 int conf manip autom robot small scales, MARSS. 2016 2016. https://doi.org/10.1109/MARSS.2016.7561698.

[30] Mok G. The design of a planar precision stage using cost effective optical mouse sensors. Technical University Delft; 2015.

[31] Lampaert SGE, Spronck JW, van Ostayen RAJ. Friction and trail formation of a planar ferrofluid bearing. Leeds-Lyon Symp. 2016. p. 4. 2016.

[32] Lampaert SGE, Spronck JW, van Ostayen RAJ, Habib H. Planar Positioning Stage with a PSD sensor and ferrofluid bearings. DSPE-Conference 2016:57–61. 2016.

[33] Van Veen S. Planar ferrofluid bearings for pecision stages. Technical University Delft; 2013.

[34] Olaru R, Petrescu C, Arcire A. Maximizing the magnetic force generated by an actuator with non-magnetic body in a ferrofluid pre-magnetized by permanent magnets. Int Rev Electr Eng 2013;8:904–11.

[35] Arcire A, Olaru R, Petrescu C. Study of the influence of ferromagnetic material on the characteristics of an actuator based on ferrofluid and permanent magnets. EPE 2012 - Proc 2012 Int Conf Expo Electr Power Eng 2012. p. 776–80. https://doi.org/10.1109/ICEPE.2012.6463838.

[36] Andersson L. Fillet away your electromagnetic field singularities. 2014.